Influence of sonocrystallization on lipid crystals multicomponent oleogels structuration and physical properties

Thais Lomonaco Teodoro da Silva[a]* and Sabine Danthine[a]

[a]Science des Aliments et Formulation, Gembloux Agro-Bio Tech, ULiège, 5030, Gembloux, Belgium

tltdsilva@uliege.be

Abstract

The use of multicomponent oleogels combined with a physical process such as high-intensity ultrasound (HIU) has become an interesting alternative to overcome nutritional and technological issues in fat-based foods. This is because the combination can add technological properties without changing the total amount of gelators, improving sensory acceptance and clean label claim. In this context, the study aims to evaluate the structuration power and physical properties of oleogels formed by monoglycerides (MG), fully hydrogenated rapessed oil (FHRO), and lecithin (LE) in rapeseed oil, with and without HIU. All samples were analyzed according to their microstructure, melting behavior, rheology, texture, polymorphism, and oil binding capacity. In mono-structured oleogels, only MG was able to form gels that did not flow. Three synergic combinations that produced 99% oil binding capacity oleogels were found: MG: FHRO, FHRO:LE, and MG:FHRO:LE. These combinations showed improved physical properties like hardness, elastic modulus, and oil loss when sonicated, which was attributed to the induced secondary crystallization of the FHRO promoted by HIU.

Keywords: multicomponent oleogels, high-intensity ultrasound, physical properties, synergism, monoglycerides, fully hydrogenated rapessed oil, lecithin.

1. Introduction

Although gelation using low-molecular-weight structuring agents has been a topic of research since the 1990s (Terech & Weiss, 1997), the nutritional appeal for "healthy fats" higher in unsaturated fatty acids and lower in saturated fatty acids has driven tremendous attention to the structured oils in the last decade. The need of “healthy fats” has created a high demand for food-grade gelators and structured oleogels with similar physical properties compared to high saturated fats. Oleogels are classified as a new class of fat replacers known as fat mimetics. Fat mimetics embrace the unsaturated oil, structured by polar lipid crystalline structure, polymeric networks of cellulose and its derivatives, emulsion-templated networks of proteins and polysaccharides, and solid emulsions of oil trapped within crystallized lamellar mesophases (Patel et al., 2020).

Oleogels, by definition, are gels formed by the addition at low concentrations (<10%) of compounds (oleogelators) to liquid oils to form a network and entrap liquid oils (Co & Marangoni, 2012). An ideal oleogelator used in food applications must be food-grade, economically viable, efficient, versatile, and match the final product's physical properties. The most studied oleogelators are vegetable waxes, fatty acids and alcohols, monoacylglycerols, phytosterols, sorbitan esters, lecithin, high melting triacylglycerols (TG), and polymers (Co & Marangoni, 2012; Dassanayake et al., 2011; Vieira et al., 2015).

The use of fat mimetics as oleogels in food-related systems has many technological/nutritional benefits, among them (1) reduction of saturated fatty acids (da Silva et al., 2018; Ferro et al., 2021), (2) minimization of oil migration (Si et al., 2016; Winkler-Moser et al., 2019), (3) increase in thermal resistance (da Silva, Arellano, et al., 2019; Stortz & Marangoni, 2013).

In order to successfully achieve these nutritionals and technological benefits, many structuration routes have been explored. Until now there is no ideal oleogelator that can achieve all physical, economical, nutritional and sensorial properties for final application, this is why multicomponents oleogels are now considered. There are three main types of multicomponents systems to obtain structuration: (1) formed by oleogelators that do not form oleogels when used alone; (2) formed by oleogelators that can form oleogels alone, forming either two different structuration routes or unic synergic one; (3) using an additive complementary to one or more oleogelators, that can improve the physical properties induced by the oleogelators alone (Vieira et al., 2015).

A second structuration route recently explored is by using high-intensity ultrasound (HIU). HIU has been used to strengthen oleogel structures and improve physical properties for monoglycerides oleogels (Giacomozzi et al., 2020; Giacomozzi et al., 2019), propolis wax oleogels (Sharifi et al., 2019), multicomponent oleogels (da Silva, Barrera, et al., 2019; da Silva & Danthine, 2021), and also to induce beeswax structuration in low concentrations (Jana & Martini, 2014). These results suggested a reduction in incompatibility and improvement in oil loss and texture, which would reduce gelator amount needed and consequently improve sensory acceptance and price. Besides, HIU as a physical process can also contribute to a clean label claim.

For these reasons, using multicomponent gelators combined with ultrasound could create interesting fat mimetics for food application. The objective of this study was to evaluate the physical properties of ternary oleogels formed by monoglycerides (MG), high melting TG (brought by fully hydrogenated rapeseed oil (FHRO)), and lecithin (LE) and their interactions, with and without sonication. By using sonicated multicomponents systems formed by

monoglycerides, high-melting point triacylgycerols (TGs), and/or lecithin, oleogelators naturally obtained from fat sources, it is expected that one or more synergic lipid mixed structured multicomponent oleogels with good physical properties for application in foods could be obtained.

2. Materials and Methods

2.1.Materials

Lecithin (LE), Lipoid P 100 (Phosphatidylcholine 90% from soybean (non-GMO)), was kindly donated by Lipoid AG (Switzerland). The typical fatty acid composition of this LE is palmitic acid (P, 12-17%), stearic acid (St, 2-5%), oleic acid (O, 7-12%), linoleic (L, 59-70%), linolenic (Ln, 5-8%). Monoglycerides (MG) Dimodan® HP MB and rapeseed oil were acquired from Royale Lacroix (Belgium). This MG is a distilled palm-based MG (≥ 90% pure), composed mainly of 56% P and 41% St (Tavernier et al., 2019). The rapeseed oil was mainly composed of triacylglycerols (TG) such as OOLn (12.1%), OOL (22.6%), OOO (29.3%), and POO (6.5%). The fully hydrogenated rapeseed oil (FHRO), formed mainly by St (92%) and P (5.5%) and consequently by StStSt (82.3%) and PStSt (14.4%) TGs, was kindly donated by Cargill (Germany).

2.2.Samples preparation

All samples were prepared to reach a total concentration of 10% (w/w) of oleogelator in the lipid phase (rapeseed oil). Oleogels were named according the gelators they contained. Three types were prepared : (1) mono-component gels with 10% of monoglycerides: MG, or 10% of fully hydrogenated rapeseed oil : FHRO, or 10% of lecithin: LE, (2) binary oleogels containing 1:1 (w:w) proportion were named as MG:FHRO, MG:LE, and FHRO:LE, and (3) the ternary combination with 1:1:1 (w:w:w) of each was named MG:FHRO:LE. The total amount of gelator

was fixed at 10% because although MG has a higher structuration power and is able to form self-sustainable gels with good physical properties within concentrations as low as 6% (Giacomozzi et al., 2019), LE and FHRO do not form gels even at 10% (Cerqueira et al., 2017; Okuro, Tavernier, et al., 2018).

Oleogels (50mL) were prepared by mixing the oleogelators in a beaker using a magnetic stirring plate set at 110°C and 350 rpm for 20 min. After complete dissolution of the gelators in the oil, the liquid oleogels were fast cooled to 55°C at ~10°C/min under low stirring (100 rpm) with a magnetic bar in a 100mL water jacket vessel (water at 55°C). Samples (50mL) were then poured into 100mL plastic containers (filling 25 cm of the 40 cm high container) and subjected to a second slow cooling step (cooling rate 0.5 °C/min), by placing the samples in an incubator set at 20 ± 0.5°C. The samples were then stored for 48h in the same incubator to stabilize the gel network at 20 ± 0.5°C (room temperature). For oleogels prepared using HIU (20kHz, CPX 750, Cole 115 PA Parmer Instruments, Illinois, USA), similar cooling steps as described for non-sonicated samples were used. HIU was placed in the middle of the water jacket vessel (2cm from the bottom) at the beginning of the fast cooling (~80 °C) when the sample was still melted. Sonication was applied only when samples reached the induction temperature (55°C) in the presence of primary nucleation for 10s using 50% amplitude (50 ± 2 W, 1W/mL). This temperature was chosen based on visual preliminary observation of the crystallization induction and from previously studies where MG and FHRO mixtures showed inductions temperatures between 56 and 40 °C (da Silva & Danthine, 2021). Moreover, the HIU conditions were chosen based on a previous work where we observed that the best moment to apply HIU was at the induction temperature. Only 10s was enough to induce secondary nucleation and improve the physical properties of oleogels (da Silva & Danthine, 2021). After sonication, samples (50mL)

were also placed in 100 mL plastic containers (filling 2.5 cm of the container) and stored in an incubator at 20 ± 0.5 °C for the second slow cooling and stored for 48h before further analysis. Oleogels with or without HIU were prepared in triplicate.

2.3.Methods

2.3.1. Microscopy

The microstructure was observed using polarized light microscopy (PLM) with an optical microscope (Nikon Eclipse E400, Kanagawa, Japan) equipped with a digital camera (Nikon, DS-FI2, Kanagawa, Japan). One drop of the stabilized sample was placed between a slide and a cover slide. Five images were collected for each oleogel sample. Ten images were selected to evaluate the crystal morphology and size using the software Image Pro-Plus (Media Cybernetics, Rockville, MD, USA). Parameters evaluated were mean diameter (Dm), crystallized area (Ca), microstructure density (De, number of microstructure unit by unit of volume), and number of crystals counted by image (Nc).

2.3.2. Oil loss

The amount of oil loss by the samples was evaluated by centrifugation with a centrifuge 5810R Eppendorf (Hamburg, Germany), according to da Silva and Danthine (2021). First, a pre-weighed empty 2mL Eppendorf (*wa*) was filled with approximately 1g of sample. The system sample + Eppendorf was weighted (*wb*) and centrifuged for 15 min at 2950g. Subsequently, the tubes were left upside down to drain the free oil for 10min. The drained Eppendorf's were weighted (*wc*). The test was performed in quadruplicate, and oil loss was calculated according to equation 1:

$$\text{Oil loss (\%)} = \left[\frac{wc-wa}{wb-wa}\right]*100 \qquad (1)$$

2.3.3. Rheology

Rheology experiments were performed at 20°C using a Modular Compact Rheometer MCR 302 (Rheoplus, Anton Paar, Austria). Plate-plate geometry with a diameter of 40mm was used with the gap set to 1000 μm. Strain sweeps were conducted from 0.0008 to 100% strain at 1Hz. The linear viscoelastic region (LVR) was calculated as the strain value where elasticity (G') was constant as the mean of LVR for G' and G''. Frequency sweeps were measured at 0.01% constant amplitude from 0.1 – 100 rad/s. The Rheoplus software (Anton Paar, Austria) was used to analyze the rheological parameters. This analysis was performed in quadruplicate.

2.3.4. Texture

A Texture Analyzer (TA-XT plus, Stable Micro Systems, UK) equipped with a 5kg load cell placed in a temperature controlled cabinet set at 20 ± 0.5 °C, was used to determine the mechanical properties of the oleogels stabilized for 48h at 20 ± 0.5 °C. A penetration test was performed using a 5-mm diameter cylinder probe: the sample was placed in the texture analyzer directly in its 100 mL container (d=6.5 cm), and was penetrated for 10mm by the probe at 1mm/s. The hardness was expressed as the maximum force of the peak (N). Analysis was performed in triplicate.

2.3.5. Melting properties

The melting curves were obtained using a Q2000 DSC (TA Instruments, New Castle, DE, USA) coupled with a refrigeration cooling system (TA Instruments, New Castle, DE, USA) and calibrated with indium and eicosane. About 5-8 mg of sample were weighted in a Tzero hermetic pan and heated from 20°C to 80°C with 5°C/min as heating rate. A similar Tzero hermetic empty pan was used as a reference, and the melting curves were analyzed using the Universal Analysis Software version 4.2 (TA Instruments, New Castle, DE, USA). The parameters evaluated were peak temperature (T_p) and enthalpy (ΔH). The analysis was performed in triplicate.

The melting point of the gelators (MG, LE, and FHRO) was also measured by DSC using a Tzero hermetically sealed pan. In this case, the samples were first heated to 100°C using a 5°C/min heating rate and kept at 100°C for 30 min to ensure complete melting; after this, they were crystallized using a 5°C/min cooling rate until -20°C and kept at this temperature for 90 min. The last step was a second melting to 100°C, at a 5°C/min heating rate. The peak temperature (T_p) obtained from the last melting step was used to quantify the melting point (Kerr et al., 2011).

2.3.6. X-ray diffraction

The powder X-ray diffraction (p-XRD) pattern was measured at 20 °C after storage at 20 °C for 48h using a Bruker D8 Advance Diffractometer (Bruker, Germany) with Cu Kα radiation (λ = 1.54178Å, 40 kV, 30 mA) with a LynxEye detector (LynxEye Bruker, Germany) at long and short spacings (1–27° 2θ) using a 0.02° step size with 135.01 s by step.

2.3.7. Statistical analysis

Oleogels with and without HIU were processed in triplicate, and all analytical measurements were performed in replicates as described above. Data shown are mean values and standard deviations of the mean. Statistical differences amongst treatments were assessed using 2-way ANOVA ($\alpha < 0.05$) that was performed using GraphPad Prism version 8.0 (La Jolla, CA). Correlation analysis was also performed using GraphPad Prism version 8.0 (La Jolla, CA).

3. Results and Discussion

3.1. Visual appearance

The macroscopic appearance of the mono, binary and ternary oleogels prepared with and without HIU were first observed (Figure 1). All the samples formed “visually structured” oleogels with macroscopically solid-like structure, except LE, FHRO, and MG:LE which stayed

liquid independently of sonication or not, as shown in Figure 1. These results were expected for LE and FHRO due to their individual low structuration power, as already described before (Cerqueira et al., 2017; Gaudino et al., 2019; Okuro, Malfatti-Gasperini, et al., 2018). On the contrary, the data obtained for MG:LE is surprising since MG alone, even in concentrations as low as 5%, which is similar to the one in the MG:LE system had a high structuration power (Ferro et al., 2019). Moreover, although LE is not a powerful oleogelator alone, requiring a higher concentration of oleogelator (>20%) (Gaudino et al., 2019), many synergic combinations of LE with other components have been reported in the literature: with sucrose esters (Sintang et al., 2017), β -sitosterol and γ-oryzanol (Okuro, Malfatti-Gasperini, et al., 2018), sorbitan tristearate (Pernetti et al., 2007), fruit wax (Okuro, Tavernier, et al., 2018) or fatty acids (Gaudino et al., 2019) for example. In those cases, the LE was not the only principal structuring agent in the network even if it co-acted with other oleogelators, forming synergic multicomponent oleogels and with improved physical properties. A similar co-acting effect probably happened in samples FHRO:LE and MG:FH:LE that formed "visually structured" samples. Samples MG and MG:FHRO also had visual solid oleogel structures. In addition, visually structured samples before sonication kept the visual structure after sonication, which suggests that HIU was been applied in an optimized condition. Sonication was previously reported to improve the appearance of low saturated fat (da Silva et al., 2021) or MG oleogels in lower concentrations of MG (3, 4.5, or 6%) (Giacomozzi et al., 2020), forming a visual more structured sample. However, in some cases, the visual appearance was also negatively affected by HIU when HIU or crystallizations conditions were not optimized (da Silva et al., 2021; da Silva & Danthine, 2021).

3.2. Melting behavior

Figure 2 shows the melting thermograms of the oleogels samples. Figure 2A shows the melting curve of the MG, FHRO, and LE. The LE is the gelator with the lowest MP, -0.75 ± 0.1 °C, followed by FHRO 61.0 ± 0.2 °C and MG with 66.5 ± 0.1 °C. The low melting point of the LE can be correlated with its fatty acid composition, mainly unsaturated fatty acids (~80%), and the higher melting point of the MG and FHRO to the very high amount of saturated fatty acids in MG (97%) and TG (100%) molecules.

The melting behavior of the oleogels can be seen in Figure 2B. MG oleogel had the highest melting parameters, represented by a higher T_{on}, $T_{p,}$ and ΔH (Table 1). HIU did not change this curve profile significantly, nor T_{on} and T_p but significantly reduced the ΔH ($p<0.05$). MG oleogels, due to the very high melting point of the gelator, showed a very fast crystallization/structuration. It is possible that HIU, instead of inducing nucleation, generated too much heat and partially melted the MG nuclei, reducing the amount of crystalline material. This is because sonication generates cavitation, which generates localized pressure and temperature increase (Wagh et al., 2016). This generally induces the nucleation (da Silva et al., 2020), nevertheless, it can also cause an opposite effect if not applied under appropriate crystallization conditions or at the appropriate moment (da Silva & Danthine, 2021). Previous results with sonication of MG oleogels using different HIU conditions such as 10s pulses or 30s with similar power level (50W) or higher (96W) and a lower concentration of MG (between 3 -6%) did not induce any change on ΔH (da Silva & Danthine, 2021; Giacomozzi et al., 2019). This suggests that the higher concentration of MG accelerated the crystallization process and that this acceleration impacted the melting energy when cavitation was applied. LE oleogels with or without HIU formed a liquid oleogel due to the low melting point of the gelator as discussed above (Figure 1) and did not show any melting peaks in the conditions of the study (>20 °C).

231 FHRO oleogels showed a melting curve at a lower temperature compared to MG oleogels, which
232 might be attributed to the lower melting point of the FHRO. There was no difference in melting
233 profile or melting parameters of FHRO oleogel due to sonication (Table 1, $p>0.05$).
234 Binary oleogels melting behavior can also be found in Figure 2B, MG:LE showed a tiny
235 and broad melting peak. The ΔH for this sample was the lowest observed. Giacomozzi et al.
236 (2019) reported that MG oleogels with 4.5% of MG, thus 0.5% less than what is added in the
237 MG:LE system, presented a much higher ΔH (~9 J/g). This suggests that LE, more than not
238 structuring by itself, also reduced the MG's structuration power, and very little crystalline
239 material was formed in this blend. HIU showed an effect on the structuration of this binary
240 blend, and a more prominent melting peak with a significantly higher enthalpy ($p<0.05$) was
241 produced. This suggested that either HIU affected the synergism of MG:LE or that LE retarded
242 MG nucleation in such a way that HIU was able to induce more crystalline material, results in
243 agreement with some previous paper on crystallization with lecithin (Cooper et al., 2019), and
244 also with optimization of HIU in MG oleogels (Giacomozzi et al., 2020). MG:FHRO oleogel
245 showed a behavior similar to both components alone, and presented a peak made of two
246 shoulders, the first at around 51°C (T_p) close to the peak of FHRO samples, and the second at
247 around 60 °C closer to MG oleogel T_p. T_p was slightly lower on both shoulders than they were
248 for the mono-component oleogels, which might indicate either eutectic or co-crystallization of
249 the components (da Silva, Arellano, et al., 2019). HIU did not induce any change in the melting
250 parameters of the MG:FHRO blend. The last binary blend evaluated was FHRO:LE oleogel
251 showed a melting curve also formed by two shoulders, which were more connected than in the
252 case of MG:FHRO, suggesting more synergism between FHRO and LE. T_p and ΔH of FHRO:LE

were significantly lower than for FHRO, and they were not affected by sonication neither ($p<0.05$).

The ternary oleogel MG:FHRO:LE showed the lowest T_{on} and T_p among all oleogels ($p<0.05$). Sonication did not change the melting parameters but slightly changed the melting profile. Without HIU MG:FHRO:LE showed one main peak with T_p at 43.2 °C, after sonication, although the prominent peak has a similar T_p (Figure 2B), a shoulder at a higher temperature was observed (~48°, see arrow). As there was no difference between ΔH with and without HIU, this process has not induced any extra crystalline material. Kadamne et al. (2017) and Lee et al. (2018) reported a fractionation for low-saturated samples crystallized in a high supercooling with ultrasound which was characterized as a shoulder at a higher temperature. Authors assumed that somehow the high-melting-point TG did not co-crystallize with the sonicated-induced lower melting points TG. In this case, the fat was structured only by TG. In the present study, the ternary oleogel possess high melting points TGs (from FHRO), MG, and phospholipids (LE). Based on the individual effect observed for the mono-component oleogels melting behavior and higher MP of MG, we could assume that MG might form this shoulder.

3.3. Microstructure

The polarized microscopy images of the samples with and without HIU are presented in Figure 3, and the parameters describing the crystals are in Table 2. MG oleogel formed small needles (2.9 μm) visually connected in an organized crystalline network. Similar morphology for a MG oleogel has been reported previously (Ferro et al., 2019; Giacomozzi et al., 2019; López-Martínez et al., 2014); nevertheless, their MG crystals were much bigger in length (Giacomozzi et al., 2020). In HIU samples, an aggregation of the needles in spherulite crystals was observed, followed by a significant increase in the mean diameter (3.5 μm). Da Silva and Danthine (2021)

observed similar needle rearrangement due to sonication which were attributed to the reduction in crystal-crystal connection in the MG crystal network of the oleogel. The sonication in the MG sample also has increased crystallized area, density, and crystals in number, suggesting that more crystals were counted, and more crystalline material was also observed. Nevertheless, this result can not be correlated with the enthalpy measured by DSC.

Although LE samples did not show a melting curve by DSC, some fiber structure could be visualized (Figure 3). Some previous studies have reported LE structuration as a 5-50 μm worm-like structure (Bodennec et al., 2016; Gaudino et al., 2019). We observed fewer and smaller fibers crystals in our study (~2.9 μm, Table 2). Usually, a minimal amount of water (<1%) was added in previous LE oleogels to increase the hydrogen bonds of the LE, strengthen the oleogel, and form an entangled network oleogel. Besides, most of the studies used higher concentrations of LE (15, 20, or 30%) (Bodennec et al., 2016; Gaudino et al., 2019). HIU in this sample has not changed the shape or improved the crystal-crystal connection but has resulted in more isolated crystals. This morphology and the low amount of crystals observed explain the liquid state in Figure 1 and confirm the low structuration power of LE alone even with sonication.

FHRO formed non-interconnected spherulites crystals without HIU (Figures 3). After sonication, increasingly interconnected crystals were observed; however, no changes in the amount of crystalline material or crystal size were found (Table 2). The crystal morphology of FHRO found has been reported before for StStSt and high StStSt fully hydrogenated oil (Barbosa et al., 2018; Cerqueira et al., 2017; da Silva, Arellano, et al., 2019).

The binary blend MG:LE, showed small needle-like crystals (2.2 μm). These needles were similar in size compared to LE and smaller than for MG. They were also not well-

299 connected, and a lot of black background representing liquid phase was visible; this explains the
300 low structuration promoted by this combination (Figure 1). This lack of structuration and much
301 lower T_p (Table 1) in this sample compared to MG samples confirms that LE is either diluting,
302 retarding, or competing with MG crystallization and preventing its structuration, a result that
303 could be attributed to the amphiphilic structure of both molecules. With HIU, the same
304 crystalline morphology was observed; nevertheless, they tend to agglomerate even more in some
305 spots looking more interconnected in some points but also with an abundant amount of black
306 background.

307 Binary blend MG:FHRO has also revealed 3µm needle-like crystals form, similar to MG
308 and FHRO alone, with a higher density of crystals and crystallized area than MG alone ($p<0.05$,
309 Table 2). HIU in this sample also formed some spherulites, similar in form and size as the MG,
310 but in a lesser amount, which might have contributed to the similar mean diameter ($p>0.05$). HIU
311 has previously shown a reorganization in the crystalline structure and complete remotion of
312 spherulites agglomeration in MG:FHRO oleogels blends when the oleogelator were used in a
313 lower concentration (6%) (da Silva & Danthine, 2021). Nevertheless, the higher concentration
314 of MG in this study seems to have avoided the same achievement.

315 The FHRO:LE oleogel has shown a very organized and connected crystal network with
316 small needles with and without HIU. Similar parameters as observed for MG:FHRO were found,
317 except for the higher number of crystals ($p<0.05$). The microstructure observed confirms a
318 synergic combination between FHRO and LE. A similar synergism was also observed between
319 LE and sorbitan tristearate (Pernetti et al., 2007), sorbitan monostearate (Sintang et al., 2017),
320 and stearic acid (Gaudino et al., 2019), suggesting that stearic acid shows a good interaction with
321 LE, not only as free fatty acid or in sorbitan ester but also in a TG form. Pernetti et al. (2007)

described this LE and stearic acid synergic combination as the LE acting as a crystal habit modifier stimulating needle or plate-shaped crystals, which are more effective in building a robust crystalline network because LE also promotes a better connection between crystals, reducing weak bonds or absence of bonds as observed in the FHRO and LE alone. Sonication even reinforces this effect because more FHRO crystallizes, induced by cavitation bubbles, resulting in an even stronger crystal network.

Interestingly, the ternary blend MG:FHRO:LE formed a combined microstructure of MG, FHRO, and LE, with needles and small spherulites. The crystalline structure formed was not very compact and interconnected when compared to the binary blends FHRO:LE and MG:FHRO, but better organized than MG:LE (Figure 3, and Table 2), which suggested that the presence of FHRO might have improved MG:LE connection. As discussed above, the LE previously showed an effective interaction with high stearic oleogelators; the MG in this study also contains palmitic acid in high amounts, which could possibly explain why they did not interact as well as in the binary FHRO:LE system which contains a majority of stearic acid. Moreover, the lack of connection between MG and FHRO could also be due to the higher amphiphilic bound present on both, creating competition between them to bound in the oil. When FHRO was added to create the ternary system, it seems to become the main building structure, and as both MG and LE can co-crystallize with the FHRO, they were all interconnected. The morphology or size of MG:FHRO:LE did not change with HIU, but the number of crystals was significantly reduced ($p<0.05$). The result was also visually observed in Figure 3. Although no changes were observed in ΔH of this sample after sonication, this effect was significant in the MG alone, and cavitation promoted by HIU might also have been too drastic for this sample.

3.4. Oil Loss

Oil loss of the oleogels can be found in Figure 4. The sample that presented the highest oil loss was LE (89.2%), followed by sample LE HIU (85.8%), and MG:LE with and without HIU (~59%). This result was expected since these samples were very liquid and not very well structured (Figures 1 and 3), and a weakly-bound oil is expected to result in more oil loss (Blake & Marangoni, 2015). Moreover, although HIU has shown significant improvement in oleogels with LE (more crystals formed), nevertheless the amount of oil lost was still very high and would compromise future (food) applications.

Samples structured by FHRO have shown intermediate oil loss values (without HIU = 38.1%) and a significant improvement was obtained with sonication (30.4%), due to the more organized crystalline network formed (Figure 3). This result confirms that network morphology strongly impacts the oil binding capacity of oleogel and sonication's positive effect in reducing oil migration in StStSt based low saturated fat (da Silva et al., 2020).

Among the visually structured samples (MG, MG:FHRO, FHRO:LE, and MG:FHRO:LE with and without HIU), MG:FHRO showed the highest oil loss (18.9%), followed by MG HIU (3.9%), all other samples with or without sonication showed oil loss lower than 1% and were statistically similar to each other ($p>0.05\%$). In summary, the oil loss results after sonication suggest that sonication generally has no effect on oil loss or a positive effect. The only case where an adverse effect was observed was in the MG sample, results in accordance with data from Giacomozzi et al. (2019, 2020) as they showed that the high saturated MGs have a very fast crystallization, including the initial nucleation. This fast nucleation challenges the application of HIU sonication at the induction time; the alternative they recommended for effectively sonicated MG oleogel was by slowing the cooling step to retard initial crystallization (Giacomozzi et al., 2020). It is important to note that this challenge on sonicated MG was not observed in binary or

ternary systems, probably because of the presence of other components which delayed the MG nucleation. This retarding in MG crystallization was already observed in a previous binary system with phytosterols (Bin Sintang et al., 2017; Truong et al., 2019). Although typically not desired, as observed for sample MG:FHRO, it benefits the sonication process, and as a consequence an improved oil binding capacity can be obtained. Previous research that investigated the effect of HIU on reducing oil migration in low saturated fat (da Silva et al., 2020) found that HIU induced the crystallization of low melting point TG that would not crystallize without the cavitation induced crystallization. The investigated oleogels are also low-saturated lipid materials, where the liquid portion was always the same in all samples (rapeseed oil in the same proportion), meaning that the main effect of HIU was on the oleogelators. In samples with FHRO, where TG drove the structuration, it is possible to relate with da Silva et al. (2020). In samples without FHRO, no observation of a self-suitainable and more structured oleogels or any improvement due to sonication could be seen, which indicated that sonication had a better effect on inducing TG than MG and LE. The addition of high-melting-point TG, even in low amounts (3.33%), improved the oleogelation process of MG, LE, and their blends.

3.5. Mechanical properties

3.5.1. Rheology

Figure 5 shows the elastic modulus (G') in a log scale of the oleogels with and without HIU obtained in the amplitude sweeps (Figure 5A) and frequency sweeps (Figure 5B). MG sample showed the highest G' (3.3 x10^5 Pa) in the linear viscoelastic region (LVR) in amplitude sweeps, followed by MG:FHRO HIU, which was significantly smaller (2.75 x 10^5 Pa, $p<0.05$). These two samples were switched in the frequency sweeps, and the highest G' found was for sample MG:FHRO HIU. FHRO:LE HIU showed the third higher G' in both analyses, a value

391 higher than the respective non-sonicated FHRO:LE sample ($p<0.05$), which was like MG HIU
392 ($p>0.05$) in amplitude sweeps.

393 It is interesting to note that HIU has shown a positive result in the elastic modulus for all
394 structured samples excepted MG, similar to what was observed for oil loss results. Even though
395 in Figure 5A we could not see the difference for some samples due to the difference in
396 magnitude between very strong oleogels and soft ones, this change promoted by HIU can be
397 observed in Figure 5B where low stress was used. Besides MG, HIU's frequency sweeps resulted
398 in a lower elasticity, and FHRO did not changed due to sonication. Ideally, fats should have a
399 shear elastic modulus between 1×10^5 –5×10^6 Pa (Patel et al., 2020). In this study, oleogels
400 MG, MG:FHRO HIU, and FHRO:LE HIU were inside this range, indicating they would be
401 suitable for fat replacement from a rheological point of view.

402 **3.5.1. Texture**

403 Hardness (Figure 6) followed a similar profile as elasticity (Figure 5A). The highest
404 hardness was found for sample MG (5N), followed by MG:FHRO HIU (3N). FHRO:LE HIU
405 was the third higher hardness (2.6N), followed by FHRO:LE without HIU (1.8N) ($p<0.05$),
406 confirming the synergic combination between the high-melting-point TG and the LE, resulting in
407 an improved hardness, elasticity, and oil binding capacity compared to the FHRO and LE alone.
408 Samples MG:HIU, MG:FHRO and MG:FHRO:LE with and without HIU, showed lower
409 hardness than others samples, but better structured than LE, FHRO and MG:LE that were
410 extremely soft regardless of sonication, confirming all the discussion above on this samples.
411 Although there is a connection between crystal network and morphology, oil loss, rheology, and
412 hardness (Blake & Marangoni, 2015), a significant Pearson correlation was found only between
413 hardness and elasticity (G') ($p<0.01$ $r=0.97$).

3.6. X-ray

X-ray diffractograms are shown in Figure 7. The pure oleogelators (MG, FHRO, and LE) are presented in Figure 7A. Small-angle X-ray scattering spectra are characterized by sharp peaks followed by weaker reflections and gives information on the crystal structure (Cerqueira et al., 2017). In that region, for MG five peaks were detected, corresponding to a lamellar distance of 47.0 Å. In the short spacings region six peaks were observed at 4.6, 4.3, 4.0, 3.8, 3.7, and 3.6 Å. The prominent peak was 4.6 Å, which indicates a polymorphism in β-form (López-Martínez et al., 2014).

Under the same conditions, the FHRO presented one major peak in the short-spacings region, observed at 4.12 Å and one main peak (50.5 Å) followed by it the reflections in the small angles region, characterizing the material as α-bilayer lamellar structure (Kodali et al., 1987).

The LE only showed peaks in the small-angle. The absence of peaks in the wide-angle was expected due to the presence of unsaturated fatty acids in the studied LE as also observed previously by other group (Li et al., 2021).

The MG oleogels showed similar long spacing region peaks as for MG alone, suggesting that there was no change in structure due to the mixture with oil. In the short spacing region, the main peaks were 4.6, 4.35, and 3.9 Å, keeping the β-form similar to MG alone. There were moreover no changes in polymorphism due to sonication, as reported before for an MG-oleogel (Giacomozzi et al., 2020).

LE-oleogels have not shown any wide-angle peaks due to the low crystallinity of the material (Aguilar-Zárate et al., 2019; Pernetti et al., 2007). Nonetheless, lamellar distance of 47.0 Å was found, a similar profile was found by Han et al. (2014), and the presence of reverse micelles in LE oleogels was indicated previously by a d-spacing as 48 Å (Gaudino et al., 2019).

Sonication in LE showed some changes, and different peaks could be observed, like 9.7, 8.2, 7.0, and 6.0 Å, besides those already observed for LE without HIU. Moreover, the peaks after sonification showed higher intensity. The higher intensity of the long spacing peaks for the oleogel prepared with soybean oil implied higher self-sorting and rearrangement of the gelator molecules, resulting in more crystals (Yang et al., 2017). The same result was also previously observed in Figure 3.

FHRO oleogels, on the other hand, showed three peaks in the wide-angle at 4.6, 4.2, and 3.8 Å, suggesting a majority of β-form. Sonication as for MG-oleogels did not change the polymorphism of the samples.

In the binary oleogels, MG:LE showed a mixed diffractogram with peaks at 4.6, 4.35, and 3.9 Å that are characteristic of MG, and peak at 47.0 Å that is characteristic of LE-oleogel. A previous blend of MG and phytosterols showed a change in the polymorphic form followed by a disruption in the pre-existing crystals compared to the gelators alone, which indicated an unstable oleogel (Zhao et al., 2020). In this case, adding the beta-sitosterol that was not structured alone in the same concentration resulted in a more viscous sample with a different polymorphic form from the MG, similar to what was observed in the MG:LE sample. In the short-spacing region, a β-form was also formed. HIU in this sample did not change the position of the peaks but strongly reduced the intensity.

MG:FHRO with or without HIU showed similar peaks, 48.0 Å was the only peak in the long spacing, and 4.6 Å was the most substantial peak at the short spacing, which was expected since this peak was predominant for MG, which also gives MG:FHRO a predominant β-form. As previously shown, HIU did not change MG:FHRO polymorphism (da Silva & Danthine, 2021).

FHRO:LE showed similar short spacing to the previous sample MG:FHRO, and consequently same polymorphic form. The small-angle showed a d-spacing at 48.0 Å, previously a combination of LE with stearic fatty acids showed a double combination of double layers (fatty acids) and reverse micelle (LE), showing two small angles patterns (Gaudino et al., 2019). In FHRO:LE, the single peak observed in the small-angle suggested that only one structure was formed.

The ternary blend showed two peaks at the small-angle region, similar to what was observed for MG and FHRO. Although peaks have a lower intensity in the short spacing, they are similar to previous samples at 4.6, 4.35, and 3.9Å, which confirms that all oleogels have a β-form, and no changes were observed due to HIU.

4. Conclusion

MG, FHRO, and LE can form synergic combinations leading to structured oleogels when in specific blends such as MG:FHRO, FHRO:LE, and MG:FHRO:LE. Although MG alone forms a very well structured and self-sustainable oleogel, with 99% oil binding capacity, these multicomponent-blends (MG:FHRO, FHRO:LE, and MG:FHRO:LE) showed a similar oil binding capacity, hardness, and viscoelasticity, but now using a much lower amount of each oleogelator. These synergic binary and ternary blends can form very interesting alternatives, mainly when HIU is applied, in such a case, they achieved a 99% oil binding capacity, which is a fundamental property for food applications. Regarding mechanical properties, the binary blends MG:FHRO and FHRO:LE showed the closest value to MG alone; although lower, they still formed oleogels with high strength and with viscoelasticity suitable for food applications. Although FHRO alone cannot provide a strong structuration, the presence of this component in the blends could help to form well-structured samples. FHRO acted either as seeding to primary

crystalline material or as a connection between MG and LE, making possible the connection of the two amphiphilic oleogelators without any water addition. Moreover, the physical properties of the binary oleogels containing FHRO were also improved by sonication. These results suggested that a small amount of high-melting-point TG can strengthen the structuration and allow cavitation to induce an even more structured oleogel. Interestingly, cavitation in the tested condition does not have the same induction effect on MG or LE, since HIU has not similarly improved them.

5. Acknowledgments

The authors are grateful for the Postdoctoral fellowships and funding in Sciences, Technology, Engineering, Materials, and Agrobiotechnology (STEMA) funding OTP Nº DIVE.0899-J-P given by ULiège University Research Council.

6. References

Aguilar-Zárate, M., Macias-Rodriguez, B. A., Toro-Vazquez, J. F., & Marangoni, A. G. (2019). Engineering rheological properties of edible oleogels with ethylcellulose and lecithin. *Carbohydrate Polymers*, *205*(October 2018), 98–105. https://doi.org/10.1016/j.carbpol.2018.10.032

Barbosa, K. M., Cardoso, L. P., Ribeiro, A. P. B., Kieckbusch, T. G., & Buscato, M. H. M. (2018). Crystallization of low saturated lipid blends of palm and canola oils with sorbitan monostearate and fully hydrogenated palm oil. *Journal of Food Science and Technology*, *55*(3), 1104–1115. https://doi.org/10.1007/s13197-017-3026-5

Bin Sintang, M. D., Rimaux, T., Van de Walle, D., Dewettinck, K., & Patel, A. R. (2017). Oil structuring properties of monoglycerides and phytosterols mixtures. *European Journal of Lipid Science and Technology*, *119*(3), 1–14. https://doi.org/10.1002/ejlt.201500517

505 Blake, A. I., & Marangoni, A. G. (2015). The Use of Cooling Rate to Engineer the
506 Microstructure and Oil Binding Capacity of Wax Crystal Networks. *Food Biophysics*, *10*,
507 456–465. https://doi.org/10.1007/s11483-015-9409-0
508 Bodennec, M., Guo, Q., & Rousseau, D. (2016). Molecular and microstructural characterization
509 of lecithin-based oleogels made with vegetable oil. *RSC Advances*, *6*(53), 47373–47381.
510 https://doi.org/10.1039/c6ra04324k
511 Cerqueira, M. A., Fasolin, L. H., Picone, C. S. F., Pastrana, L. M., Cunha, R. L., & Vicente, A.
512 A. (2017). Structural and mechanical properties of organogels: Role of oil and gelator
513 molecular structure. *Food Research International*, *96*, 161–170.
514 https://doi.org/10.1016/j.foodres.2017.03.021
515 Co, E. D., & Marangoni, A. G. (2012). Organogels: An alternative edible oil-structuring method.
516 *Journal of the American Oil Chemists' Society*, *89*, 749–780.
517 https://doi.org/10.1007/s11746-012-2049-3
518 Cooper, Z., Simons, C., & Martini, S. (2019). Retardation of Crystallization through the Addition
519 of Dairy Phospholipids. *JAOCS, Journal of the American Oil Chemists' Society*, *96*(11),
520 1205–1218. https://doi.org/10.1002/aocs.12269
521 da Silva, T. L. T., Arellano, D. B., & Martini, S. (2019). Interactions between candelilla wax and
522 saturated triacylglycerols in oleogels. *Food Research International*, *121*, 900–909.
523 https://doi.org/10.1016/j.foodres.2019.01.018
524 da Silva, T. L. T., Barrera, D. A., & Martini, S. (2019). Use of High-Intensity Ultrasound to
525 Change the Physical Properties of Oleogels and Emulsion Gels. *Journal of American Oil*
526 *Chemistry Society*, *96*, 681–691. https://doi.org/10.1002/aocs.12215
527 da Silva, T. L. T., Chaves, K. F., Fernandes, G. D., Rodrigues, J. B., Bolini, H. M. A., &

Arellano, D. B. (2018). Sensory and Technological Evaluation of Margarines With Reduced Saturated Fatty Acid Contents Using Oleogel Technology. *Journal of American Oil Chemistry Society*, *95*(6), 673–685. https://doi.org/10.1002/aocs.12074

da Silva, T. L. T., Cooper, Z., Lee, J., Gibon, V., & Martini, S. (2020). Tailoring Crystalline Structure Using High-Intensity Ultrasound to Reduce Oil Migration in a Low Saturated Fat. *Journal of American Oil Chemists' Society*, *97*, 141–155. https://doi.org/10.1002/aocs.12321

da Silva, T. L. T., & Danthine, S. (2021). Effect of high-intensity ultrasound on the oleogelation and physical properties of high melting point monoglycerides and triglycerides oleogels. *Journal of Food Science*, *86*(2), 343–356. https://doi.org/10.1111/1750-3841.15589

da Silva, T. L. T., Danthine, S., & Martini, S. (2021). Palm-based fat crystallized at different temperatures with and without high-intensity ultrasound in batch and in a scraped surface heat exchanger. *LWT - Food Science and Technology*, *138*, 110593. https://doi.org/10.1016/j.lwt.2020.110593

Dassanayake, L. S. K., Kodali, D. R., & Ueno, S. (2011). Formation of oleogels based on edible lipid materials. *Current Opinion in Colloid and Interface Science*, *16*, 432–439. https://doi.org/10.1016/j.cocis.2011.05.005

Ferro, A. C., de Souza Paglarini, C., Rodrigues Pollonio, M. A., & Lopes Cunha, R. (2021). Glyceryl monostearate-based oleogels as a new fat substitute in meat emulsion. *Meat Science*, *174*(December 2020), 108424. https://doi.org/10.1016/j.meatsci.2020.108424

Ferro, A. C., Okuro, P. K., Ribeiro, A. P. badan, & Cunha, R. L. (2019). Role of the oil on glyceryl monostearate based oleogels. *Food Research International*, *120*, 610–619. https://doi.org/10.1016/j.foodres.2018.11.013

551 Gaudino, N., Ghazani, S. M., Clark, S., Marangoni, A. G., & Acevedo, N. C. (2019).
552 Development of lecithin and stearic acid based oleogels and oleogel emulsions for edible
553 semisolid applications. *Food Research International*, *116*(December 2018), 79–89.
554 https://doi.org/10.1016/j.foodres.2018.12.021
555 Giacomozzi, A., Palla, C., Carrin, M. E., & Martini, S. (2020). Tailoring physical properties of
556 monoglycerides oleogels using high- intensity ultrasound. *Food Research International*,
557 *134*(April), 109231. https://doi.org/10.1016/j.foodres.2020.109231
558 Giacomozzi, A. S., Palla, C. A., Carr, E., & Martini, S. (2019). Physical Properties of
559 Monoglycerides Oleogels Modified by Concentration , Cooling Rate , and High-Intensity
560 Ultrasound. *Journal of Food Science*, *84*(9), 2549–2561. https://doi.org/10.1111/1750-
561 3841.14762
562 Han, L., Li, L., Li, B., Zhao, L., Liu, G. Q., Liu, X., & Wang, X. (2014). Structure and physical
563 properties of organogels developed by sitosterol and lecithin with sunflower oil. *JAOCS,*
564 *Journal of the American Oil Chemists' Society*, *91*(10), 1783–1792.
565 https://doi.org/10.1007/s11746-014-2526-y
566 Jana, S., & Martini, S. (2014). Effect of high-intensity ultrasound and cooling rate on the
567 crystallization behavior of beeswax in edible oils. *Journal of Agricultural and Food*
568 *Chemistry*, *62*(41), 10192–10202. https://doi.org/10.1021/jf503393h
569 Kadamne, J. V., Ifeduba, E. A., Akoh, C. C., & Martini, S. (2017). Sonocrystallization of
570 Interesterified Fats with 20 and 30% of Stearic Acid at the sn-2 Position and Their Physical
571 Blends. *Journal of the American Oil Chemists' Society*, *94*(8), 1045–1062.
572 https://doi.org/10.1007/s11746-017-3014-y
573 Kerr, R. M., Tombokan, X., Ghosh, S., & Martini, S. (2011). Crystallization Behavior of

574 Anhydrous Milk Fat - Sunflower Oil Wax Blends. *Journal of Agricultural and Food*
575 *Chemistry*, *59*, 2689–2695. https://doi.org/doi/abs/10.1021/jf1046046
576 Kodali, D. R., Atkinson, D., Redgrave, T. G., & Small, D. M. (1987). Structure and
577 polymorphism of 18-carbon fatty acyl triacylglycerols: Effect of unsaturation and
578 substitution in the 2-position. *Journal of Lipid Research*, *28*(4), 403–413.
579 https://doi.org/10.1016/s0022-2275(20)38692-2
580 Lee, J., Claro da Silva, R., Gibon, V., & Martini, S. (2018). Sonocrystallization of Interesterified
581 Soybean Oil: Effect of Saturation Level and Supercooling. *Journal of Food Science*, *83*(4),
582 902–910. https://doi.org/10.1111/1750-3841.14084
583 Li, J., Yu, H., Yang, Y., Drummond, C. J., & Conn, C. E. (2021). Effect of Crystallization State
584 on the Gel Properties of Oleogels Based on β-sitosterol. *Food Biophysics*, *16*(1), 48–57.
585 https://doi.org/10.1007/s11483-020-09648-6
586 López-Martínez, A., Morales-Rueda, J. A., Dibildox-Alvarado, E., & Charó-Alonso, M. A.
587 (2014). Comparing the crystallization and rheological behavior of organogels developed by
588 pure and commercial monoglycerides in vegetable oil. *Food Research Internation*, *64*, 946–
589 957. https://doi.org/10.1016/j.foodres.2014.08.029
590 Okuro, P. K., Malfatti-Gasperini, A. A., Vicente, A. A., & Cunha, R. L. (2018). Lecithin and
591 phytosterols-based mixtures as hybrid structuring agents in different organic phases. *Food*
592 *Research International*, *111*, 168–177. https://doi.org/10.1016/j.foodres.2018.05.022
593 Okuro, P. K., Tavernier, I., Sintang, D. Bin, Skirtach, A. G., Vicente, A. A., Dewettinck, K., &
594 Cunha, R. L. (2018). Synergistic interactions between lecithin and fruit wax in oleogel
595 formation. *Food & Function*, *9*, 1755–1767. https://doi.org/10.1039/c7fo01775h
596 Palla, C., de Vicente, J., Carrín, M. E., & Gálvez Ruiz, M. J. (2019). Effects of cooling

temperature profiles on the monoglycerides oleogel properties: A rheo-microscopy study. *Food Research International*, *125*, 108613. https://doi.org/10.1016/j.foodres.2019.108613

Patel, A. R., Nicholson, R. A., & Marangoni, A. G. (2020). Applications of fat mimetics for the replacement of saturated and hydrogenated fat in food products. *Current Opinion in Food Science*, *33*, 61–68. https://doi.org/10.1016/j.cofs.2019.12.008

Pernetti, M., van Malssen, K., Kalnin, D., & Fl??ter, E. (2007). Structuring edible oil with lecithin and sorbitan tri-stearate. *Food Hydrocolloids*, *21*(5–6), 855–861. https://doi.org/10.1016/j.foodhyd.2006.10.023

Sharifi, M., Goli, S. A. H., & Fayaz, G. (2019). Exploitation of high-intensity ultrasound to modify the structure of olive oil organogel containing propolis wax. *International Journal of Food Science and Technology*, *54*, 509–515. https://doi.org/10.1111/ijfs.13965

Si, H., Cheong, L. Z., Huang, J., & Wang, X. (2016). Physical Properties of Soybean Oleogels and Oil Migration Evaluation in Model Praline System. *Journal of the American Oil Chemists' Society*, *93*, 1075–1084. https://doi.org/10.1007/s11746-016-2846-1

Sintang, M. D. Bin, Danthine, S., Patel, A. R., Rimaux, T., Walle, D. Van De, & Dewettinck, K. (2017). Mixed surfactant systems of sucrose esters and lecithin as a synergistic approach for oil structuring. *Journal of Colloid And Interface Science*, *504*, 387–396. https://doi.org/10.1016/j.jcis.2017.05.114

Stortz, T. A., & Marangoni, A. G. (2013). Ethylcellulose solvent substitution method of preparing heat resistant chocolate. *Food Research International*, *51*, 797–803. https://doi.org/10.1016/j.foodres.2013.01.059

Tavernier, I., Moens, K., Heyman, B., Danthine, S., & Dewettinck, K. (2019). Relating crystallization behavior of monoacylglycerols-diacylglycerol mixtures to the strength of

their crystalline network in oil. *Food Research International*, *120*(November 2018), 504–513. https://doi.org/10.1016/j.foodres.2018.10.092

Terech, P., & Weiss, R. G. (1997). Low molecular mass gelators of organic liquids and the properties of their gels. *Chemical Reviews*, *97*(8), 3133–3159. https://doi.org/10.1021/cr9700282

Truong, T., Prakash, S., Bhandari, B., & EU. (2019). Effects of crystallisation of native phytosterols and monoacylglycerols on foaming properties of whipped oleogels. *Food Chemistry*, *285*(September 2018), 86–93. https://doi.org/10.1016/j.foodchem.2019.01.134

Vieira, S. A., McClements, D. J., & Decker, E. A. (2015). Challenges of utilizing healthy fats in foods. *Advances in Nutrition*, *6*, 309S-317S. https://doi.org/10.3945/an.114.006965

Wagh, A., Birkin, P., & Martini, S. (2016). High-Intensity Ultrasound to Improve Physical and Functional Properties of Lipids. *Annual Review of Food Science and Technology*, *7*(1), 23–41. https://doi.org/10.1146/annurev-food-041715-033112

Winkler-Moser, J. K., Anderson, J., Byars, J. A., Singh, M., & Hwang, H. S. (2019). Evaluation of Beeswax, Candelilla Wax, Rice Bran Wax, and Sunflower Wax as Alternative Stabilizers for Peanut Butter. *Journal of the American Oil Chemists' Society*, *96*(11), 1235–1248. https://doi.org/10.1002/aocs.12276

Yang, S., Li, G., Saleh, A. S. M., Yang, H., Wang, N., Wang, P., Yue, X., & Xiao, Z. (2017). Functional Characteristics of Oleogel Prepared from Sunflower Oil with β-Sitosterol and Stearic Acid. *Journal of the American Oil Chemists' Society*, *94*(9), 1153–1164. https://doi.org/10.1007/s11746-017-3026-7

Zhao, M., Lan, Y., Cui, L., Monono, E., Rao, J., & Chen, B. (2020). Physical properties and cookie-making performance of oleogels prepared with crude and refined soybean oil: A

comparative study. *Food and Function*, *11*(3), 2498–2508.

https://doi.org/10.1039/c9fo02180a

Figure Captions

Figure 1. Visual appearance of mono, bi, and ternary oleogels formed by monoglycerides (MG), fully hydrogenated rapeseed oil (FHRO), and lecithin (LE) at 20°C, with and without high-intensity ultrasound (HIU).

Figure 2. Melting point (A) of the gelators monoglycerides (MG), fully hydrogenated rapeseed oil (FHRO), and lecithin (LE) and melting behavior (B) of mono, bi, and ternary oleogels formed by MG, HF, and LE, with (dashed lines) and without (direct lines) high-intensity ultrasound (HIU).

Figure 3. Polarized light images obtained from mono, bi, and ternary oleogels formed by monoglycerides (MG), fully hydrogenated rapeseed oil (FHRO), and lecithin (LE) at 20°C, with and without high-intensity ultrasound (HIU).

Figure 4. Oil loss (%) of mono, bi, and ternary oleogels formed by monoglycerides (MG), fully hydrogenated rapeseed oil (FHRO), and lecithin (LE) at 20°C, with and without high-intensity ultrasound (HIU).

Figure 5. Elastic modulus obtained as a mean of the linear region in the amplitudes sweeps (A) and elastic modulus profile in the frequency sweeps (B) for the mono, bi, and ternary oleogels formed by monoglycerides (MG), fully hydrogenated rapeseed oil (FHRO), and lecithin (LE) at 20°C, with and without high-intensity ultrasound (HIU).

Figure 6. Hardness (N) of the mono, bi, and ternary oleogels formed by monoglycerides (MG), fully hydrogenated rapeseed oil (FHRO), and lecithin (LE) at 20°C, with and without high-intensity ultrasound (HIU).

Figure 7. X-ray diffraction pattern for gelators (A) and oleogels (B, C) mono, bi, and ternary structured by monoglycerides (MG), fully hydrogenated rapeseed oil (FHRO), and lecithin (LE) at 20°C, with and without high-intensity ultrasound (HIU).

Table 1: Melting parameters of mono, bi, and ternary oleogels formed by monoglycerides (MG), fully hydrogenated rapeseed oil (FHRO), and lecithin (LE), with and without high-intensity ultrasound (HIU).

Samples	**T_{on} (°C)	T_p (°C)	ΔH (J/g)
MG	56.3 ± 0.4 [a*]	64.7 ± 0.8 [a]	18.1 ± 1.6 [a]
MG HIU	56.1 ± 1.0 [a]	63.8 ± 1.0 [a]	14.4 ± 2.1 [b]

LE	-	-	-
LE HIU	-	-	-
FHRO	46.3 ± 1.9 ^{b}	55.5 ± 1.0 ^{b}	15.6 ± 1.1 ^{ab}
FHRO HIU	46.4 ± 0.5 ^{b}	55.1 ± 0.3 ^{b}	15.6 ± 0.7 ^{ab}
MG:LE	41.7 ± 1.8 ^{b}	50.3 ± 0.4 ^{de}	1.9 ± 1.4 ^{e}
MG:LE HIU	32.4 ± 4.5 ^{c}	49.4 ± 0.3 ^{ef}	5.5 ± 1.4 ^{d}
MG:HF	46.5 ± 0.4 ^{b}	52.3 ± 0.1 ^{c}	16.6 ± 2.0 ^{ab}
MG:FHRO HIU	42.7 ± 1.3 ^{b}	51.8 ± 0.9 ^{cd}	17.0 ± 1.4 ^{ab}
FHRO:LE	39.8 ± 1.1 ^{b}	48.2 ± 1.3 ^{f}	7.9 ± 0.7 ^{cd}
FHRO:LE HIU	40.1 ± 1.0 ^{b}	48.1 ± 0.2 ^{f}	9.3 ± 0.2 ^{c}
MG:FHRO:LE	31.9 ± 2.1 ^{c}	43.2 ± 0.9 ^{g}	6.6 ± 2.1 ^{cd}
MG:FHRO:LE HIU	33.2 ± 0.8 ^{c}	42.5 ± 0.6 ^{g}	7.6 ± 0.6 ^{cd}

673 * Samples followed by the same letter in the same column are not statistically different from each other based on Tukey test (α=0.05).** Ton:
674 onset temperature, Tp: peak temperature, ΔH: enthalpy

675

676 **Table 2:** Crystal diameter (Dm), crystallized area (CA), density (De), and the number of the
677 crystals counted (Nc) for each sample.

Samples	Dm (µm)	CA (%)	De	Nc
MG**	*2.9 ± 0.2 ^{bc}	0.8 ± 0.2 ^{f}	133.3 ± 10.8 ^{d}	2171.6 ± 280.7 ^{de}
MG HIU	3.5 ±0.5 ^{a}	1.6 ± 0.2 ^{c}	157.4 ± 6.4 ^{c}	2582.3 ± 772.4 ^{d}
LE	2.5 ± 0.1 ^{bcd}	0.4 ± 0.1 ^{g}	176.7 ± 4.6 ^{ab}	1988.5 ± 91.8 ^{de}
LE HIU	3.8 ± 0.5 ^{a}	0.1 ± 0.1 ^{g}	181.7 ± 5.0 ^{a}	262.3 ± 98.1 ^{e}
FHRO	2.9 ± 0.2 ^{bc}	1.7 ± 0.2 ^{bc}	152.3 ± 8.2 ^{c}	3505.3 ± 636.7 ^{cd}
FHRO HIU	2.9 ± 0.2 ^{bc}	1.7 ± 0.2 ^{bc}	156.4 ± 10.7 ^{c}	5930.8 ± 1203.6 ^{ab}
MG:LE	2.2 ± 0.1 ^{d}	2.0 ± 0.1 ^{ab}	147.8 ± 5.5 ^{c}	4858.0 ± 1507.7 ^{abc}
MG:LE HIU	2.1 ± 0.1 ^{d}	2.1 ± 0.2 ^{a}	151.4 ± 5.5 ^{cd}	3192.0 ± 1046.6 ^{cd}
MG:HF	3.0 ± 0.4 ^{b}	1.7 ± 0.1 ^{c}	150.4 ± 6.4 ^{c}	3430.2 ± 1467.0 ^{cd}
MG:FHRO HIU	3.0 ± 0.5 ^{b}	1.6 ± 0.2 ^{c}	149.5 ± 7.0 ^{c}	2802.4 ± 1407.6 ^{d}
FHRO:LE	2.6 ± 0.2 ^{bcd}	1.5 ± 0.1 ^{c}	144.6 ± 13.1^{cd}	6388.0 ± 2099.5 ^{a}
FHRO:LE HIU	2.8 ± 0.2 ^{bc}	1.6 ± 0.1 ^{cd}	154.8 ± 5.3 ^{c}	5644.1 ± 1114.8 ^{ab}
MG:FHRO:LE	2.3 ± 0.2 ^{cd}	1.2 ± 0.3 ^{de}	160.7 ± 4.1 ^{bc}	7132.0 ± 1194.4 ^{a}
MG:FHRO:LE HIU	2.3 ± 0.3 ^{c}	1.1 ± 0.3 ^{ef}	156.8 ± 19.4 ^{c}	4045.5 ± 1207.6 ^{bcd}

678 * Samples followed by the same letter in the same column are not statistically different from each other based on Tukey test (α=0.05). **MG:
679 monoglycerides, LE: lecithin, FHRO: fully hydrogenated rapeseed oil and their blends with high-intensity ultrasound (HIU) or without.

Figures Captions

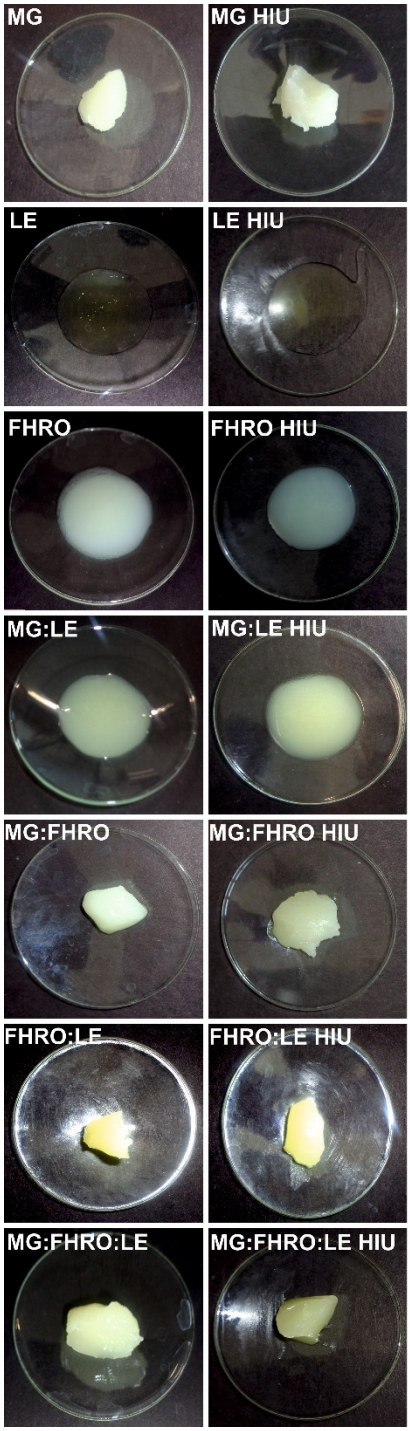

Figure 1. Visual appearance of mono, bi, and ternary oleogels formed by monoglycerides (MG), fully hydrogenated rapeseed oil (FHRO), and lecithin (LE) at 20°C, with and without high-intensity ultrasound (HIU).

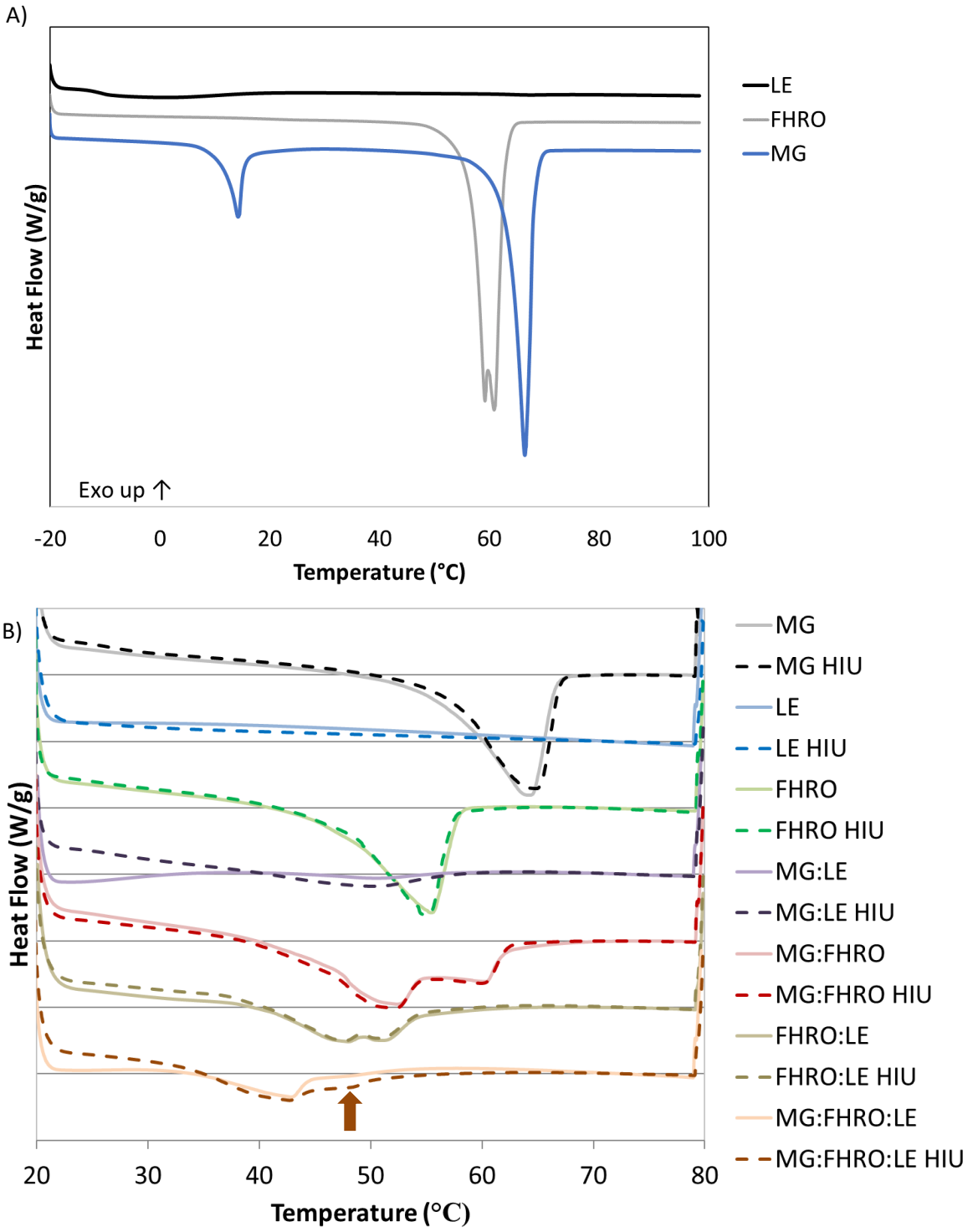

686 **Figure 2.** Melting point (A) of the oleogelators monoglycerides (MG), fully hydrogenated
687 rapeseed oil (FHRO), and lecithin (LE) and melting behavior (B) of mono, bi, and ternary
688 oleogels formed by MG, HF, and LE, with (dashed lines) and without (direct lines) high-
689 intensity ultrasound (HIU).

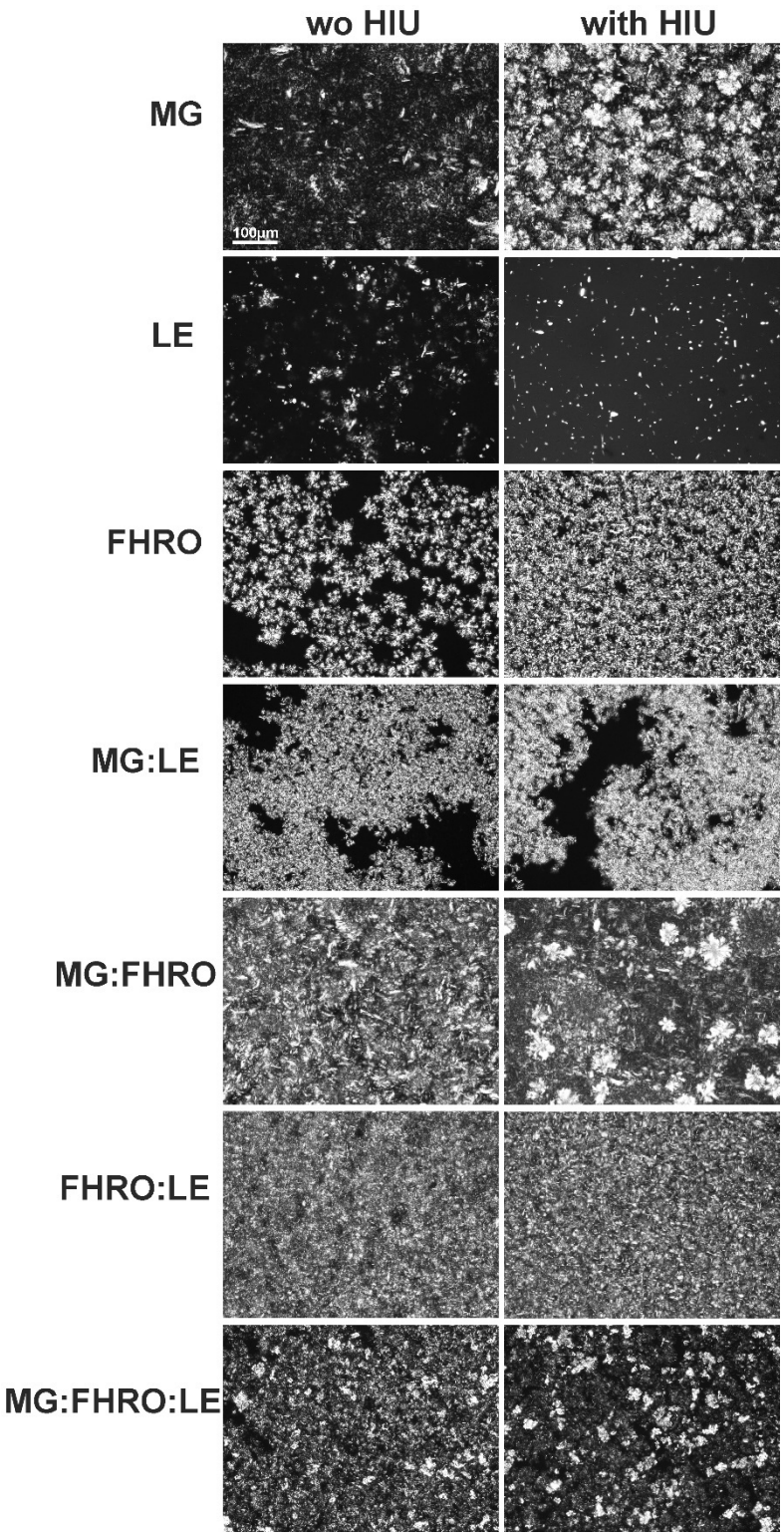

690

691 **Figure 3.** Polarized light images obtained from mono, bi, and ternary oleogels formed by monoglycerides
692 (MG), fully hydrogenated rapeseed oil (FHRO), and lecithin (LE) at 20°C, with and without high-
693 intensity ultrasound (HIU).

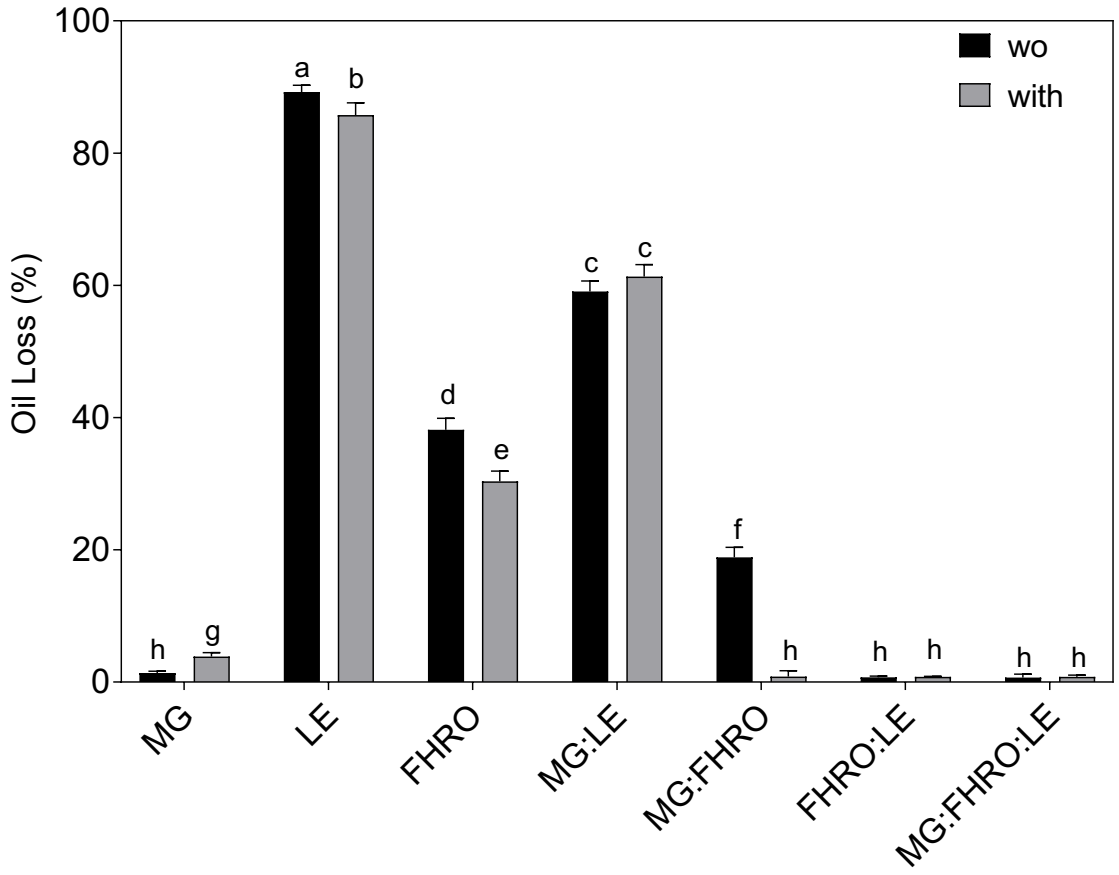

694

695 **Figure 4.** Oil loss (%) of mono, bi, and ternary oleogels formed by monoglycerides (MG), fully
696 hydrogenated rapeseed oil (FHRO), and lecithin (LE) at 20°C, with and without high-intensity
697 ultrasound (HIU).

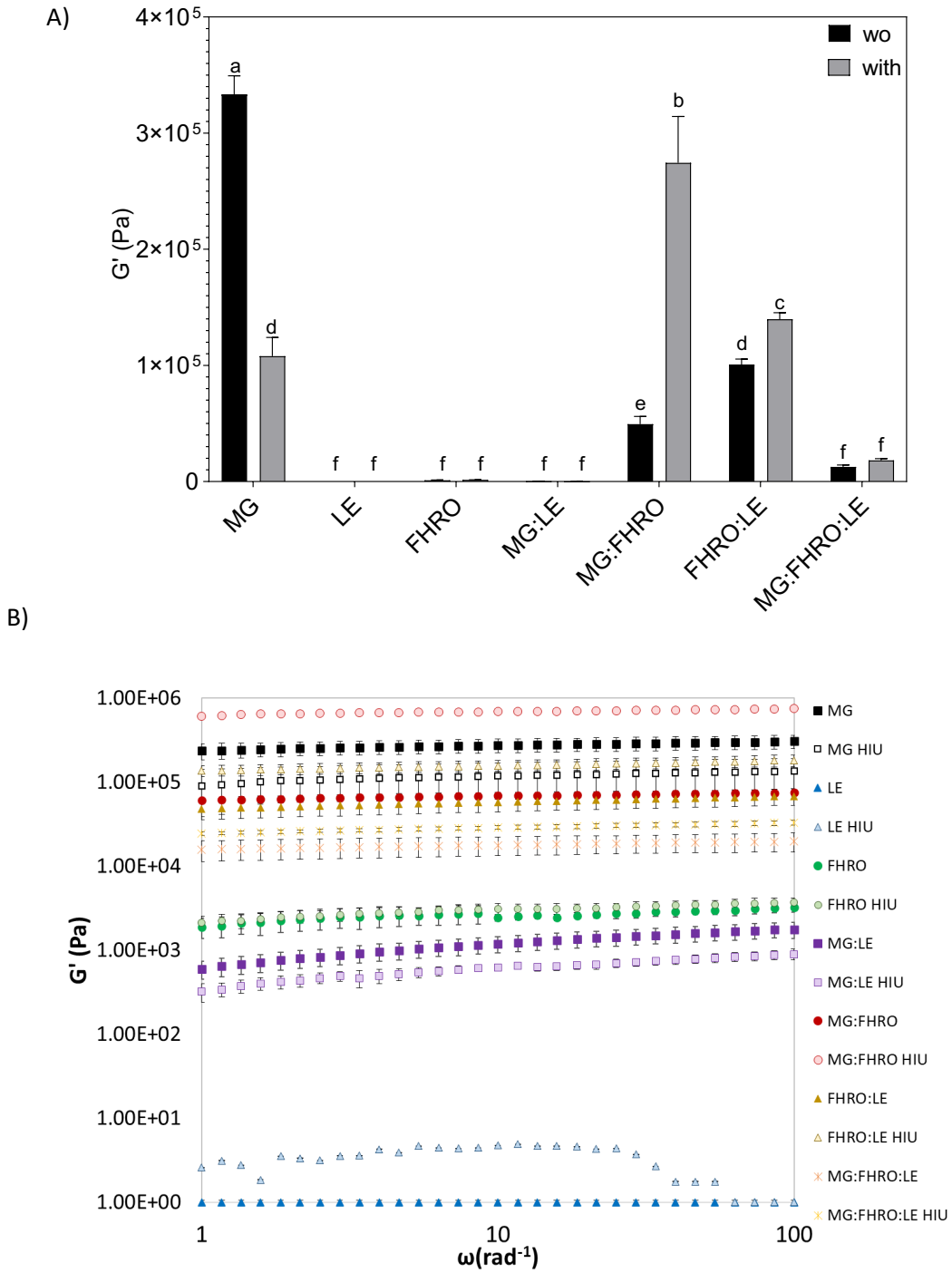

Figure 5. Elastic modulus obtained as a mean of the linear region in the amplitudes sweeps (A) and elastic modulus profile in the frequency sweeps (B) for the mono, bi, and ternary oleogels formed by monoglycerides (MG), fully hydrogenated rapeseed oil (FHRO), and lecithin (LE) at 20°C, with and without high-intensity ultrasound (HIU).

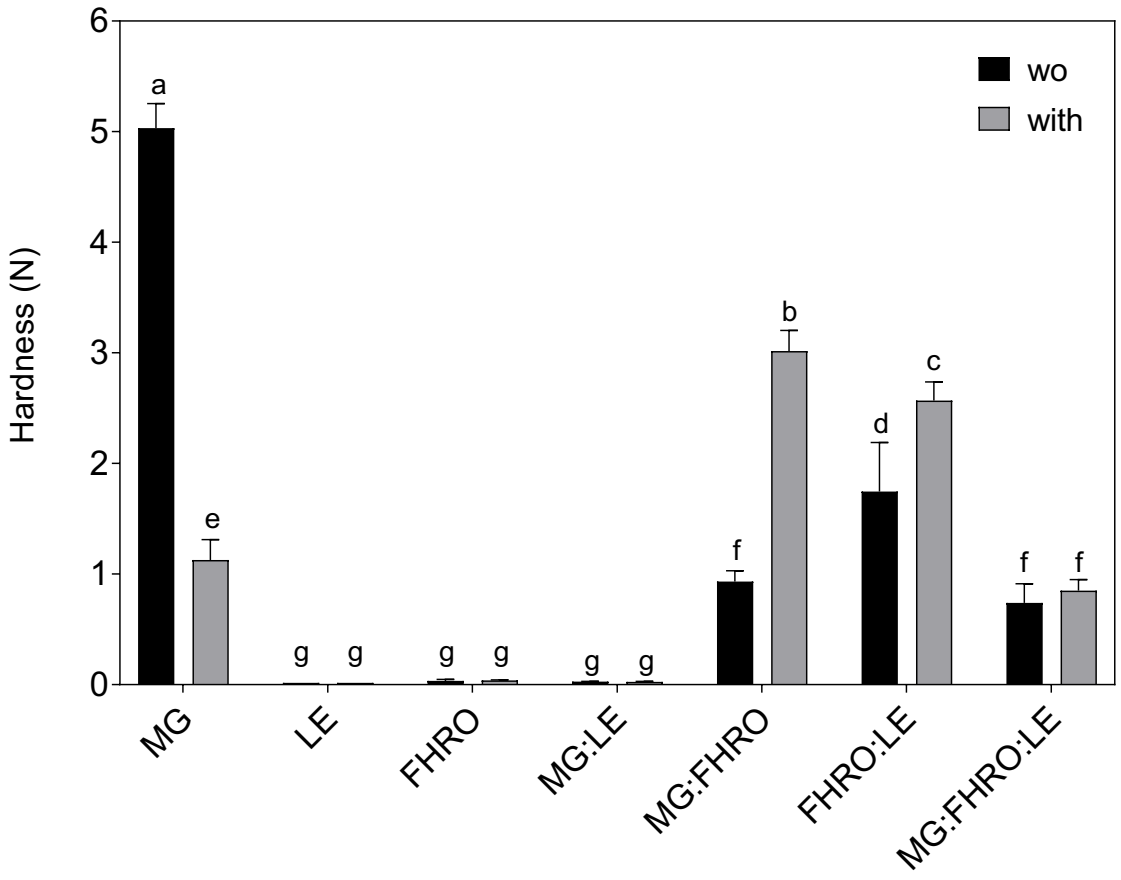

Figure 6. Hardness (N) of the mono, bi, and ternary oleogels formed by monoglycerides (MG), fully hydrogenated rapeseed oil (FHRO), and lecithin (LE) at 20°C, with and without high-intensity ultrasound (HIU).

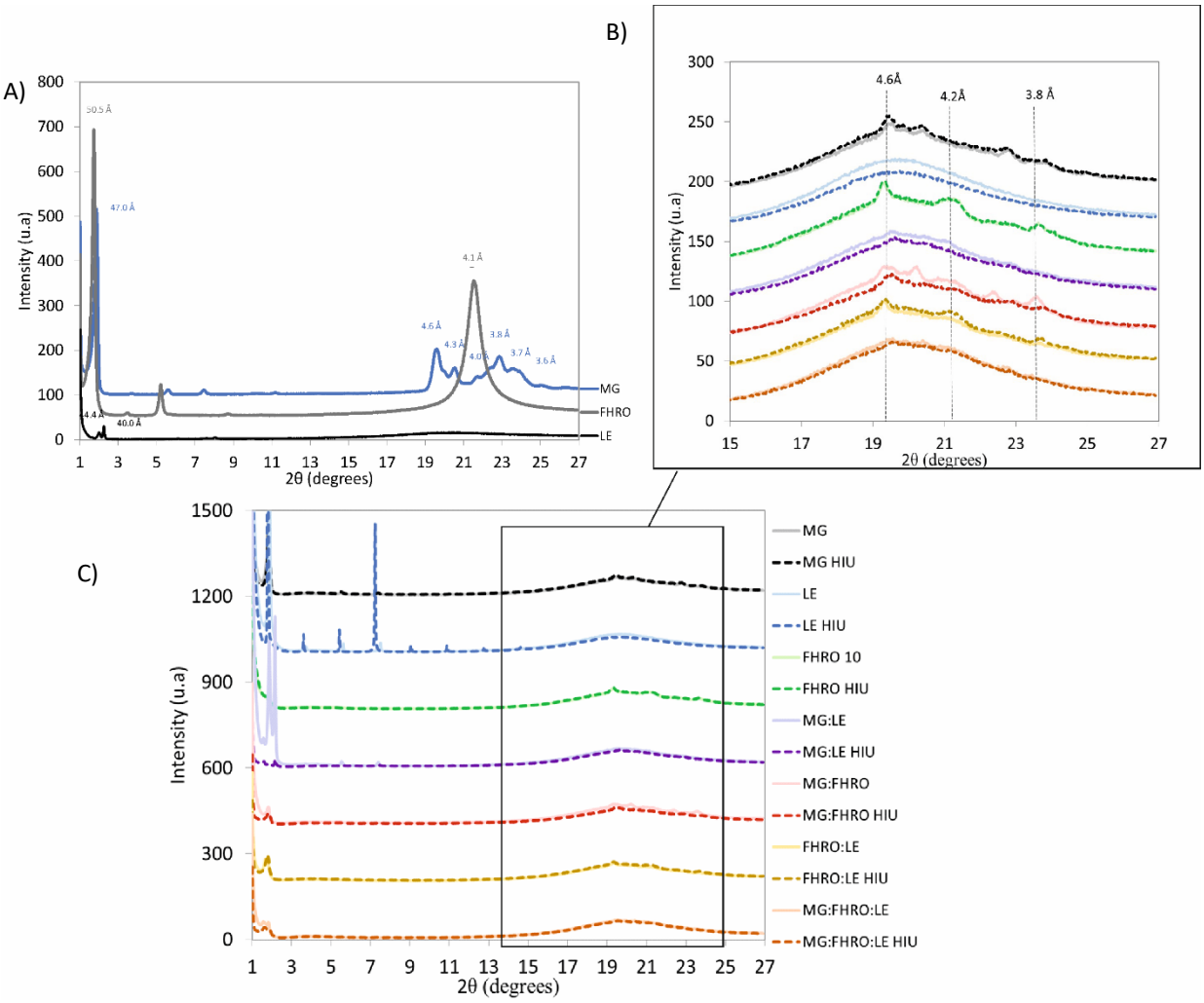

Figure 7. X-ray diffraction pattern for gelators (A) and oleogels (B, C) mono, bi, and ternary structured by monoglycerides (MG), fully hydrogenated rapeseed oil (FHRO), and lecithin (LE) at 20°C, with and without high-intensity ultrasound (HIU).